Journal of Sound and Vibration (2001) **246**(1), 97–113
doi:10.1006/jsvi.2000.3609, available online at http://www.idealibrary.com on IDEAL®

NUMERICAL EXPERIMENTS ON ACOUSTIC RECIPROCITY IN COMPRESSIBLE POTENTIAL FLOWS IN DUCTS

W. EVERSMAN

Mechanical and Aerospace Engineering and Engineering Mechanics, University of Missouri-Rolla, Rolla, MO 65401, *U.S.A.*

(*Received* 8 *May* 2000, *and in final form* 21 *December* 2000)

A reciprocity theorem for the scattering matrix for the propagation of acoustic modes in a duct with acoustically hard walls or with acoustically absorbing walls has been given in a companion publication. It was found that for a source at a specified end of the duct, suitably scaled reflection matrices in direct and reverse flow have a reciprocal relationship. Scaled transmission matrices obtained for direct flow and reversed flow with simultaneous switching of source location from one end to the other also have a reciprocal relationship. A reverse flow theorem for the equivalent one-dimensional propagation model, which is a good approximation to the three-dimensional model at low frequencies, was also obtained. In this case, using reciprocity and acoustic power conservation arguments it is additionally found that the acoustic power transmission coefficient is the same for a source at either end of the duct for a given flow direction. This result leads to an invariance theorem which relates acoustic power propagated due to sources of equal pressure amplitude at the two ends of the duct. A numerical verification of these reciprocal relationships is given here for propagation in axially symmetric (circular and annular) ducts with multi-modal propagation and at low frequencies when a one-dimensional model is appropriate.

1. INTRODUCTION

In a companion paper [1], a reverse flow reciprocity theorem has been developed for acoustic propagation in non-uniform ducts carrying compressible mean flow. In the general case of multi-mode propagation, reciprocity relations for scattering coefficients are shown for ducts with either rigid walls or with walls which include a normally reacting, dissipative section. For a source at one end of the duct, scaled reflection matrices in direct and reverse flow have a reciprocal relationship. Scaled transmission matrices obtained for direct flow and reversed flow with simultaneous switching of source location from one end to the other also have a reciprocal relationship. Reciprocity is also shown for the long wavelength approximation when a one-dimensional model is applicable. In this case, acoustic treatment is not part of the model. Results similar to the multi-modal case are established for reciprocal relationships for reflection and transmission coefficients. Additional results which are part of a general power transmission invariance principal are also found as a result of reciprocity and energy conservation. This invariance principal contains as a special case a result found by Davis [2].

The reverse flow reciprocity theorem is developed directly from an integral relationship based on the acoustic field equations, using an approach similar to that used in reference [3] in the case of propagation in a non-uniform duct in the absence of flow. In particular, the

0022-460X/01/360097 + 17 $35.00/0

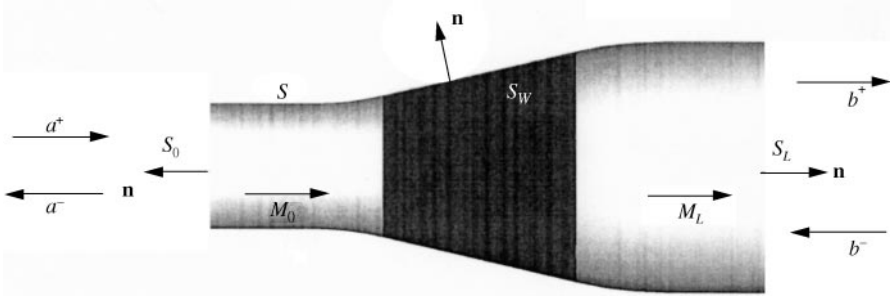

Figure 1. An x, r slice of a non-uniform duct showing acoustic treatment, uniform extensions, acoustic modal amplitudes, and relevant surfaces and surface normals.

development does not begin with an energy principle. This is in distinction to the approach of Moehring [4, 5]. The major complication which arises in the present formulation is the case when a portion of the duct wall is acoustically treated with a normally reacting dissipative lining. The boundary condition of Myers [6] is manipulated, using identities of vector calculus suggested by Moehring [5], to make it possible to establish reciprocity in this case.

The reverse flow reciprocity theorem is developed in detail in reference [1] and the results are briefly summarized here. Figure 1 shows a non-uniform duct section bounded on either end by uniform sections (long enough to have essentially uniform flow so that acoustic propagation can be synthesized in terms of duct modes). At the two ends of the duct, the acoustic field is the superposition of modes propagating to the right and to the left (including cut-off modes which technically do not propagate, but which can be segregated into right and left modes). Amplitudes a_n^+ and a_n^- refer to right and left modes at the end $x = 0$ and b_n^+ and b_n^- refer to right and left modes at $x = L$. a^+, a^-, b^+, b^-, are vectors of modal amplitudes. These modal amplitudes are related by the scattering matrix $[S]$ according to

$$\begin{Bmatrix} a^- \\ b^+ \end{Bmatrix} = [S] \begin{Bmatrix} a^+ \\ b^- \end{Bmatrix}. \tag{1}$$

The scattering matrix is defined as

$$[S] = \begin{bmatrix} [R] & [\tilde{T}] \\ [T] & [\tilde{R}] \end{bmatrix}. \tag{2}$$

Contained in $[S]$ are the usual reflection matrix $[R]$ and transmission matrix $[T]$ for acoustic modes incident at $x = 0$ and reflection and transmission matrices $[\tilde{R}]$ and $[\tilde{T}]$ for modes incident at $x = L$. In multi-modal propagation, the scattering matrix relates all modes which are considered. In the case of one-dimensional propagation (the long wavelength approximation), the scattering matrix relates only two modal amplitudes at each end. The reflection and transmission matrices are scalars, defined as reflection and transmission coefficients.

In the context of reversed flow reciprocity, there is a scattering matrix $[S_1]$ for nominal mean flow and a second one $[S_2]$ for reversed flow. It is the relationship between $[S_1]$ and $[S_2]$ which is considered in references [1, 2]. Modal amplitudes in the present discussion are in terms of acoustic potential duct modes, because the acoustic field equations are naturally in terms of acoustic potential. Equivalent results are obtained in references [1, 2] for

acoustic pressure modal amplitudes and it is only necessary at this point to refer to the properties of the acoustic potential scattering matrices.

The reverse flow reciprocity principle is

$$[S_1]^{\mathrm{T}}[J][\alpha] = [J][\alpha][S_2] \tag{3}$$

or

$$[J][\alpha][S_1] = ([J][\alpha][S_2])^{\mathrm{T}}. \tag{4}$$

The diagonal matrices $[J]$ and $[\alpha]$ are scaling matrices which have elements depending on the mode considered. The evaluation of these matrices is covered in detail in reference [1].

Equations (3) and (4) show that a weighted version of the nominal flow acoustic potential scattering matrix and similarly weighted version of the reversed flow acoustic potential scattering matrix are transposes of one another. In terms of the acoustic potential reflection and transmission coefficient matrices the result is

$$[R_1]^{\mathrm{T}}[J_0][\alpha_0] = [J_0][\alpha_0][R_2], \qquad [\tilde{R}_1]^{\mathrm{T}}[J_L][\alpha_L] = [J_L][\alpha_L][\tilde{R}_2], \tag{5, 6}$$

$$[T_1]^{\mathrm{T}}[J_L][\alpha_L] = [J_0][\alpha_0][\tilde{T}_2], \qquad [\tilde{T}_1]^{\mathrm{T}}[J_0][\alpha_0] = [J_L][\alpha_L][T_2]. \tag{7, 8}$$

Subscripts 0 and L refer to the evaluation of the relevant scaling coefficients at the two ends $x = 0$ and L. The reciprocal relationships of equations (5)–(8) involve acoustic potential reflection and transmission coefficient matrices, with diagonal elements representing reflection and transmission coefficients in the incident modes (here referred to as direct reflection or transmission) and off-diagonal reflection and transmission coefficients from the incident mode to another mode. Equations (5) and (6) show that direct acoustic potential reflection coefficients are invariant in reversed flow. The transmission coefficient matrix pairs $[T_1]$, $[T_2]$ and $[\tilde{T}_1]$, $[\tilde{T}_2]$ are not reciprocally related but the pairs $[T_1]$, $[\tilde{T}_2]$ and $[\tilde{T}_1]$, $[T_2]$ are related by equations (7) and (8). The notation convention uses the subscripts 1 and 2 to denote flow direction (1 being nominal, 2 being reversed). Tilde, or lack thereof denotes source location (tilde denoting source location reversal).

In the one-dimensional approximation [1] the same reciprocal relations apply, but in a simplified form. Reflection coefficients in nominal and reversed flow are invariant:

$$R_1 = R_2, \qquad \tilde{R}_1 = \tilde{R}_2. \tag{9, 10}$$

Scaled transmission coefficients are invariant to simultaneous flow reversal and source plane reversal:

$$T_1 A_L \frac{\rho_{r_L}}{c_{r_L}} = \tilde{T}_2 A_0 \frac{\rho_{r_0}}{c_{r_0}}, \qquad T_2 A_L \frac{\rho_{r_L}}{c_{r_L}} = \tilde{T}_1 A_0 \frac{\rho_{r_0}}{c_{r_0}}. \tag{11, 12}$$

In the case of one-dimensional propagation, there are additional results which can be deduced based on reciprocity and energy conservation. Power transmission coefficients T_π are defined as the ratio of transmitted power to incident power. It is found that

$$T_{\pi_1} = T_{\pi_2} = \tilde{T}_{\pi_1} = \tilde{T}_{\pi_2}. \tag{13}$$

Here, as in the previous discussion, the subscripts 1 and 2 refer to flow direction and the tilde or lack thereof refers to source location. Power transmission coefficients are invariant to flow reversal and source location reversal. That is, the power transmission coefficient is the same for flow in either direction, for a source at either end of the duct. Power reflection coefficients R_π are defined as the ratio of reflected power to incident power. It is also

found that

$$R_{\pi_1} = R_{\pi_2} = \tilde{R}_{\pi_1} = \tilde{R}_{\pi_2}. \tag{14}$$

Power reflection coefficients are invariant to flow reversal and source location reversal.

The results summarized by equations (5)–(14) are interesting theoretically and also provide useful benchmarks which can be used to validate propagation calculations. In the following sections two finite element codes for duct propagation, one multi-modal and the other one-dimensional, are used to demonstrate several of these reciprocal relations.

2. ACOUSTIC PROPAGATION IN A COMPRESSIBLE POTENTIAL FLOW

Reciprocity relations previously described will be verified by computations based on two FEM codes for duct propagation, one for multi-modal propagation and the other specialized for one-dimensional propagation. In this section, only a brief description of the multi-modal propagation code will be given. Details of the FEM modelling approach can be found in references [7, 8].

A formulation in terms of acoustic potential is used to produce a weak formulation suitable for finite element discretization to reduce the field equations to a single scalar variable. The geometry of the duct in Figure 1, and the steady flow field is axially symmetric. The acoustic field is not axially symmetric but is represented as azimuthally periodic in a cylindrical co-ordinate system with x being the axis of symmetry, r the cylindrical radius in a circular cross-section at $x = 0$, and θ the angular co-ordinate. Solutions are sought in angular harmonics of a Fourier Series in θ enumerated by the angular mode number m. This reduces the solution domain to a two-dimensional x, r plane, shown in Figure 1. The duct shape in a θ = constant plane shows the surface S which defines the duct shape and could include an inner surface for an annular duct. Part of S includes S_w, which is a locally reacting acoustic treatment.

The acoustic field is assumed to be harmonic in time at non-dimensional frequency η_r. Geometry is non-dimensional based on a reference length generally chosen as the radius of the inlet at the source plane, R. Acoustic and steady flow variables are non-dimensional based on reference values of the speed of sound and density of the medium, ρ_∞, c_∞, generally defined at the plane of the acoustic source. The non-dimensional frequency is $\eta_r = \omega R/c_\infty$, with ω the harmonic source frequency.

Field equations for continuity and momentum and the isentropic equation of state are used in a weighted residual statement to obtain an integral formulation which is then written in discrete form using standard FEM procedures. In terms of acoustic potential, the weak formulation is

$$\int\int_V \int \frac{\rho_r}{c_r^2} \{c_r^2 \nabla W \cdot \nabla\phi - (\mathbf{V}_r \cdot \nabla W)(\mathbf{V}_r \cdot \nabla\phi) + \mathrm{i}\eta_r [W(\mathbf{V}_r \cdot \nabla\phi) - (\mathbf{V}_r \cdot \nabla W)\phi] - \eta_r^2 W\phi\} \,\mathrm{d}V$$

$$= \int_S \int \frac{\rho_r}{c_r^2} \{c_r^2 W \nabla\phi - \mathbf{V}_r W (\mathbf{V}_r \cdot \nabla\phi) - \mathrm{i}\eta_r \mathbf{V}_r W\phi\} \cdot \mathbf{n} \,\mathrm{d}S, \tag{15}$$

where the local non-dimensional steady flow velocity is $\mathbf{V}_r = \nabla\phi_r$, with ϕ_r the non-dimensional steady flow velocity potential. The local non-dimensional density and speed of sound are ρ_r, c_r. The surface integral on the right-hand side introduces the noise source and termination conditions on S_0 or S_L and a possible impedance boundary condition on S inside the duct. In the present investigation, it is the impedance boundary condition which is of interest on S_w, a portion of S. In equation (15), the weighted residuals

statement, W, represents an arbitrary weighting function selected from the class of continuous functions. In this weak formulation the approximation to the solution ϕ is also chosen from the class of continuous functions.

At a duct wall the mean flow is tangential to the wall and $\mathbf{V}_r \cdot \mathbf{n} = 0$ causing the boundary integral (the contribution to the right-hand side of equation (1) related to the impedance condition) to become

$$I_b = \int_{S_w} \int \rho_r W \nabla \phi \cdot \mathbf{n} \, \mathrm{d}S. \tag{16}$$

It is shown in reference [9] that at a wall of admittance A, the weighted residual boundary integral of equation (16) on the duct surface S_w, derived from the Myers boundary condition [7], is

$$I_b = -\int_{S_w} \int A\rho_r^2 \{\mathrm{i}\eta_r W\phi + W\mathbf{V}_r \cdot \nabla\phi - \phi\mathbf{V}_r \cdot \nabla W - \frac{1}{\mathrm{i}\eta_r}(\mathbf{V}_r \cdot \nabla W)(\mathbf{V}_r \cdot \nabla\phi)\} \, \mathrm{d}S. \tag{17}$$

An accurate representation of this impedance boundary condition is essential to obtaining verification of reciprocal relationships when acoustic treatment is inserted into the duct wall [9]. References [7, 8] deal with propagation and radiation to the far field from open-ended ducts. In the code described here, rather than model radiation to the far field from the open end, non-reflecting boundary conditions are imposed at the termination. The boundary integral of equation (15) is used to introduce the source (at either end of the duct) as a superposition of acoustic potential duct modes and to implement the non-reflecting boundary condition based on another superposition of duct modes. The one-dimensional code is based on the one-dimensional field equations [1], and therefore has no provision for acoustic treatment. Other details of this code are similar to the multi-modal code. In both cases, the steady mean flow field which is the required data for propagation calculations is provided by an FEM potential flow code which introduces compressibility by iteration of successive incompressible flow problems. Steady flow is produced on the acoustic FEM mesh for convenience of data transfer.

The FEM codes provide solutions for the acoustic potential field which is post-processed to obtain acoustic pressure. Included as part of the solution are the acoustic potential modal amplitudes a^+, a^-, b^+, b^-. These are also converted to acoustic pressure modal amplitudes. Additional post-processing produces computations of acoustic power and power reflection and transmission coefficients.

3. NUMERICAL EXPERIMENTS ON RECIPROCITY

The first numerical verification of the reciprocal characteristics of the scattering matrix for an axially symmetric duct has been carried out in the case of a duct with a transition from annular to circular, as shown in an x, r slice in Figure 2. The interior contour is that of a typical turbofan inlet and the uniform extensions are added to meet the requirements of the present analysis (uniform flow and proper definition of acoustic eigenfunctions). The finite element mesh used in the computations is shown in this figure and is typical for examples cited here. The conditions for the "nominal" case are standard atmospheric conditions at the source plane ($x = 0$), Mach number at the source plane $M_0 = 0{\cdot}27$, directed left to right (opposite to the direction in an inlet). The non-dimensional frequency (based on the source plane) is $\eta_r = 10$. In the nominal case, the input plane for scattering is the source plane at $x = 0$. Figure 3 shows isopotential contours for the steady compressible flow in the duct which varies roughly between $M = 0{\cdot}27$ and $0{\cdot}15$. Figure 3 is unaltered in

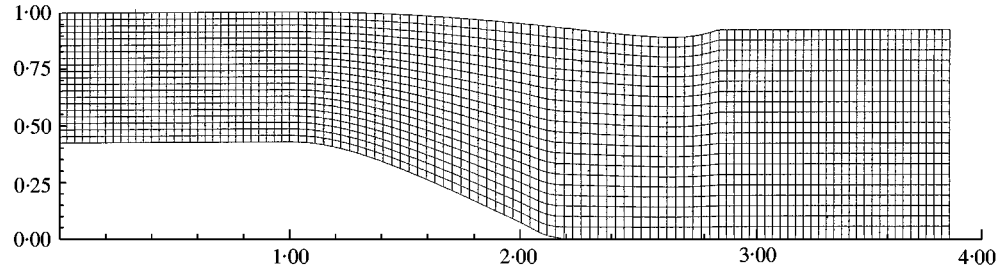

Figure 2. Plane section through the axis of a duct which has a transition from annular to circular, showing the duct profile and a typical finite element mesh.

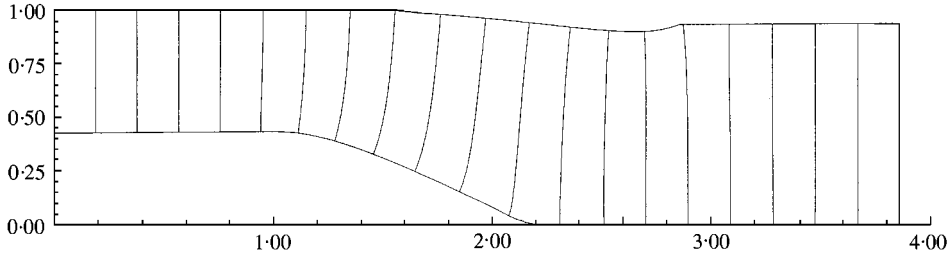

Figure 3. Iso-potential contours for steady flow through the annular/circular duct.

form for reverse flow (right to left and in the direction expected in an inlet). The acoustic analysis is based on input modes with angular dependence $m = 3$, for which there exist two propagating modes at each end of the duct ($n = 1, 2$). The third mode, $n = 3$, is cut off at both ends of the duct with cut-off ratio $\xi = 0{\cdot}87$ at $x = 0$ and $0{\cdot}84$ at $x = L$. Two cases of duct wall characteristics are studied. In the first case, the duct walls are acoustically hard, that is the impedance is infinite and the admittance vanishes. In the second case, the outer duct wall is acoustically treated from $x = 1{\cdot}0$ through 80% of the non-uniform section. The impedance is chosen as $Z = 2{\cdot}0–1{\cdot}0\mathrm{i}$, which is not optimum for attenuation for the given conditions, but is not untypical for aircraft applications. The acoustic power attenuation with the simplest radial mode incident ($m = 3$, $n = 1$) is about 9 dB, so there is a significant decrease in acoustic power from one end of the duct to the other, attributable to the wall treatment.

To generate the scaled reflection and transmission coefficient matrices in this case, input modes $n = 1$, 2 and 3 are considered. This produces 3×3 matrices which include two propagating modes and one mode which is cut off at both ends. To build the reflection and transmission matrices to verify equations (5) and (7), it is required to consider nine propagation cases: three input modes at $x = 0$ for nominal flow; three input modes at $x = 0$ for reverse flow; and three input modes at $x = L$ for reverse flow.

Reference to contours of equal acoustic pressure provide evidence of the differences induced by varying the source mode number, source location and the flow direction. Figure 4 shows acoustic iso-pressure contours for the duct with acoustic treatment when the input radial mode at $x = 0$ is $n = 1$. There is significant scattering and this is verified by reference to the scattering coefficients. Figure 5 shows the case of a mode $n = 3$ input at $x = L$ in reverse flow. This mode is cut off at both ends, and it should be noted how rapidly the acoustic pressure level is attenuated away from the source plane.

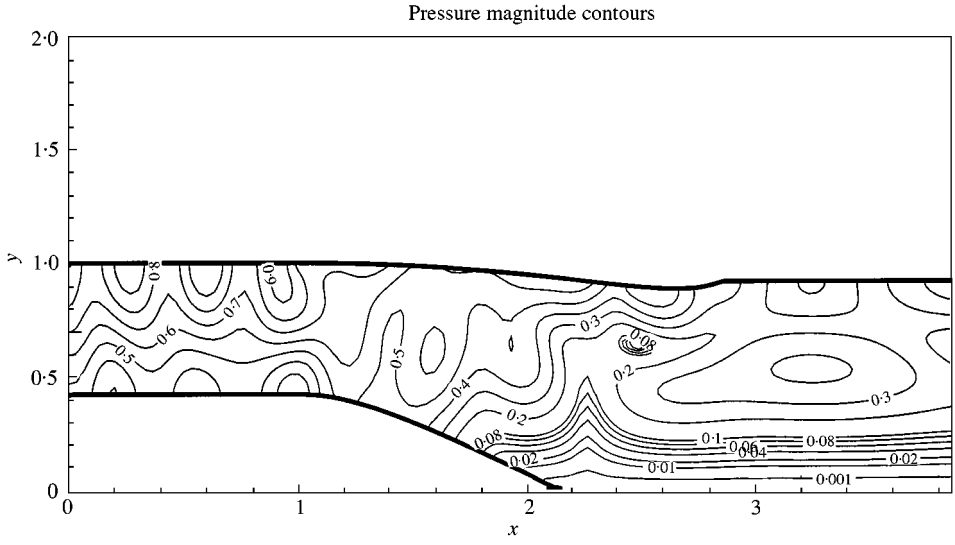

Figure 4. Acoustic iso-pressure contours for acoustically treated annular/circular duct with nominal flow. At $x = 0$ the Mach number is $M_0 = 0{\cdot}27$, the non-dimensional frequency is $\eta_r = 10{\cdot}0$, and the input mode on the left is $m = 3$, $n = 1$. Contours are typical for a well cut on input mode.

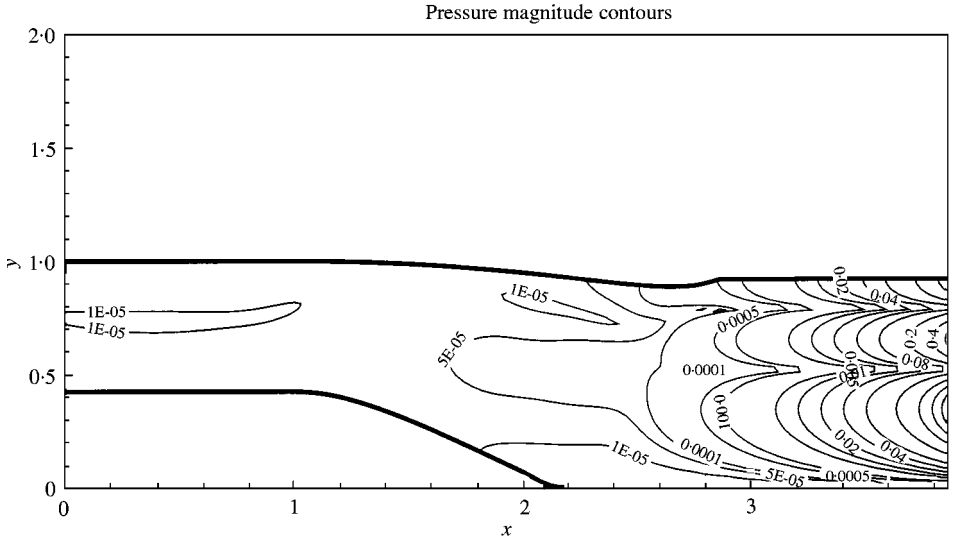

Figure 5. Acoustic iso-pressure contours for acoustically treated annular/circular duct with reverse flow. At $x = 0$ the Mach number is $M_0 = -0{\cdot}27$, the non-dimensional frequency is $\eta_r = 10{\cdot}0$, and the input mode on the right is $m = 3$, $n = 3$. Contours are typical for a moderately cut off input mode.

Table 1 shows the scaled acoustic potential reflection coefficient matrix in nominal flow with the scattering plane (acoustic source plane) at $x = 0$, which corresponds to the left-hand side of equation (5). Table 2 is the reflection matrix at $x = 0$ in reversed flow, corresponding to the right-hand side of equation (5). Equation (5) predicts that these

TABLE 1

Scaled acoustic potential reflection coefficients for nominal flow and source at $x = 0$ for the transition from an annular to circular hard wall duct which corresponds to the left-hand side of equation (5). $\eta_r = 10$, $m = 3$

Mode	1	2	3
1	− 0·14380 − 0·03098 i	− 0·13986 + 0·07217 i	− 0·153(− 4) − 0·549(− 5) i
2	− 0·13746 + 0·71323 i	− 0·04113 + 0·20572 i	0·104(− 3) + 0·732(− 5) i
3	− 0·424(− 5) + 0·841(− 5) i	− 0·144(− 4) − 0·903(− 4) i	− 0·682(− 5) + 0·497(− 8) i

TABLE 2

Scaled acoustic potential reflection coefficients for reverse flow and source at $x = 0$ for the transition from an annular to circular hard wall duct which corresponds to the right-hand side of equation (5). $\eta_r = 10$, $m = 3$

Mode	1	2	3
1	− 0·14380 − 0·03098 i	− 0·13746 + 0·71323 i	− 0·424(− 5) + 0·841(− 5) i
2	− 0·13986 + 0·07217 i	− 0·04113 + 0·20572 i	− 0·144(− 4) − 0·903(− 8) i
3	− 0·153(− 4) − 0·549(− 5) i	− 0·104(− 3) + 0·732(− 5) i	− 0·682(− 5) + 0·497(− 8) i

TABLE 3

Scaled acoustic potential transmission coefficients for nominal flow and source at $x = 0$ for the transition from an annular to circular hard wall duct which corresponds to the left-hand side of equation (7). $\eta_r = 10$, $m = 3$

Mode	1	2	3
1	− 4·12246 + 0·00532 i	− 0·56880 + 0·23281 i	0·151(− 4) − 0·109(− 4) i
2	0·58902 + 0·37376 i	− 1·74565 − 0·27580 i	0·834(− 4) + 0·174(− 4) i
3	0·300(− 4) − 0·897(− 4) i	− 0·169(− 3) + 0·105(− 3) i	0·808(− 8) − 0·488(− 8) i

TABLE 4

Scaled acoustic potential transmission coefficients for reverse flow and source at $x = L$ for the transition from an annular to circular duct which corresponds to the right-hand side of equation (7). $\eta_r = 10$, $m = 3$

Mode	1	2	3
1	− 4·12246 + 0·00532 i	0·58902 + 0·37376 i	− 0·300(− 4) − 0·897(− 4) i
2	− 0·56880 + 0·23821 i	− 1·74565 − 0·27580 i	− 0·169(− 3) − 0·105(− 3) i
3	0·151(− 4) − 0·109(− 4) i	0·834(− 4) + 0·174(− 4) i	0·808(− 8) − 0·488(− 8) i

TABLE 5

Scaled acoustic potential reflection coefficients for direct flow and source at $x = 0$ for the transition from an annular to circular acoustically treated duct which corresponds to the left-hand side of equation (5). $\eta_r = 10$, $m = 3$

Mode	1	2	3
1	0·16904 − 0·23900 i	− 0·12975 − 0·18014 i	− 0·482(− 3) − 0·677(− 4) i
2	− 0·07368 − 0·10133 i	− 0·00984 − 0·03495 i	− 0·275(− 3) + 0·950(− 4) i
3	− 0·305(− 3) + 0·632(− 5) i	− 0·283(− 3) + 0·556(− 5) i	− 0·693(− 5) + 0·510(− 6) i

TABLE 6

Scaled acoustic potential reflection coefficients for reverse flow and source at $x = 0$ for the transition from an annular to circular acoustically treated duct which corresponds to the right-hand side of equation (5). $\eta_r = 10$, $m = 3$

Mode	1	2	3
1	0·16904 − 0·23900 i	− 0·07368 − 0·10133 i	− 0·305(− 3) + 0·632(− 5) i
2	− 0·12975 − 0·18014 i	− 0·00984 − 0·03495 i	− 0·283(− 3) + 0·556(− 5) i
3	− 0·482(− 3) − 0·677(− 4) i	− 0·275(− 3) + 0·950(− 4) i	− 0·693(− 5) + 0·510(− 6) i

TABLE 7

Scaled acoustic potential transmission coefficients for direct flow and source at $x = 0$ for the transition from an annular to circular acoustically treated duct which corresponds to the left-hand side of equation (7). $\eta_r = 10$, $m = 3$

Mode	1	2	3
1	− 1·21549 + 0·02495 i	− 0·25788 + 0·60030 i	0·780(− 4) − 0·227(− 3) i
2	0·38577 − 0·37557 i	− 0·76395 + 0·24663 i	0·146(− 3) − 0·741(− 4) i
3	− 0·319(− 4) − 0·753(− 4) i	− 0·532(− 4) + 0·849(− 4) i	0·109(− 7) − 0·205(− 7) i

TABLE 8

Scaled acoustic potential transmission coefficients for reverse flow and source at $x = L$ for the transition from an annular to circular acoustically treated duct which corresponds to the left-hand side of equation (7). $\eta_r = 10$, $m = 3$

Mode	1	2	3
1	− 1·21549 + 0·02495 i	0·38577 − 0·37557 i	− 0·319(− 4) − 0·753(− 4) i
2	− 0·25788 + 0·60030 i	− 0·76395 + 0·24663 i	− 0·532(− 4) + 0·849(− 4) i
3	0·780(− 4) − 0·227(− 3) i	0·146(− 3) − 0·741(− 4) i	0·109(− 7) − 0·205(− 7) i

matrices should be reciprocals of one another. Tables 1 and 2 verify this with exceptional accuracy.

Tables 3 and 4 verify the prediction of equation (7). Table 3 gives the scaled acoustic potential transmission coefficients in nominal flow with the source at $x = 0$. Table 4 gives the scaled transmission coefficients in reversed flow with the source shifted to $x = L$. Equation (7) predicts a reciprocal relationship which is accurately substantiated in Tables 3 and 4. A point of interest in the results shown in Tables 1–4 is that reciprocity extends to cut-off modes in which case the power transmission is only accounted for by interaction of left and right modes.

Tables 5–8 are for the case with acoustic treatment in place. Table 5 shows the scaled acoustic potential reflection coefficient matrix in nominal flow with the scattering plane (acoustic source plane) at $x = 0$, and with the non-uniform portion of the duct outer wall acoustically treated. This corresponds to the left-hand side of equation (5). Table 6 is the reflection matrix at $x = 0$ in reversed flow, corresponding to the right-hand side of equation (5) for the same acoustic treatment configuration. Equation (5) predicts that these matrices should be reciprocals of one another. Tables 5 and 6 verify this, again with exceptional accuracy.

Tables 7 and 8 verify the prediction of equation (7) in the case of an acoustically treated outer wall. Table 7 gives the scaled acoustic potential transmission coefficients in direct flow with the source at $x = 0$. Table 8 gives the scaled transmission coefficients in reversed flow with the source shifted to $x = L$. Equation (7) predicts a reciprocal relationship which is accurately substantiated in Tables 7 and 8. Again, the applicability of the reciprocity principle to cut-off modes is verified.

The next case considered involves a steady flow in which the Mach number becomes relatively high, emphasizing the dependence of the acoustic treatment boundary condition on Mach number. An additional complication introduced here is the segmenting of the acoustic treatment into two equal length parts with different impedances, spanning the entire transition section. A continuous transition occurs within one element of the FEM mesh. The impedances in this case are $Z_1 = 2{\cdot}0–1{\cdot}0\,\mathrm{i}$ and $Z_2 = 3{\cdot}0–2{\cdot}0\,\mathrm{i}$ (numbered left to right). This satisfies the requirement of the reciprocity theorem and also simulates a near discontinuity of impedance. Here, a converging duct with a contraction ratio of $\sigma = 0{\cdot}5$, as shown in Figure 6, accelerates the flow (iso-potential contours are shown in Figure 6) from a Mach number at the nominal source plane of $M = 0{\cdot}13$ to $M = 0{\cdot}71$ at the exit plane. An acoustic propagation analysis has been carried out for the non-dimensional frequency $\eta_r = 10$ for a source with angular mode $m = 3$. In this geometry, and the resulting steady flow there are two propagating modes at $x = 0$ (determined in the hard wall case), but just one propagating mode at $x = L$. Results for scaled potential reflection and

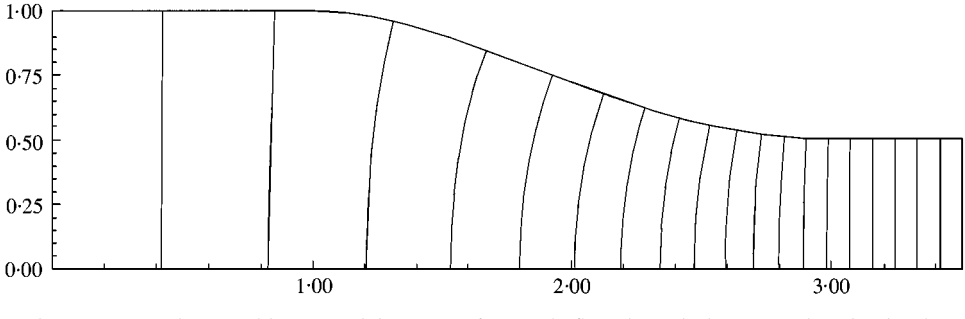

Figure 6. Duct shape and iso-potential contours for steady flow through the converging circular duct.

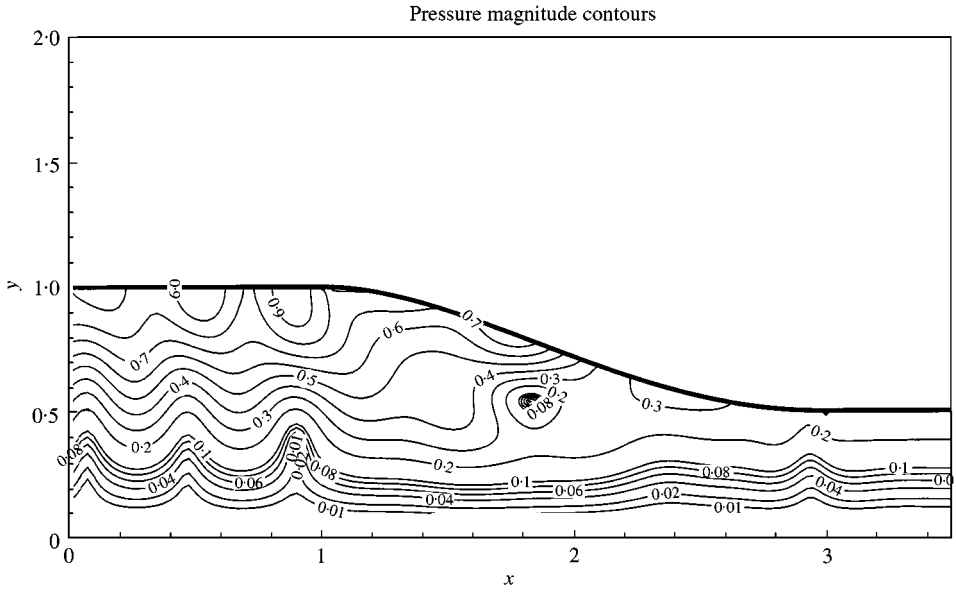

Figure 7. Acoustic iso-pressure contours for acoustically treated converging circular duct with nominal flow. At $x = 0$ the Mach number is $M_0 = -0{\cdot}13$ and at $x = L$ the Mach number is $M_L = -0{\cdot}71$. The non-dimensional frequency is $\eta_r = 10{\cdot}0$, and the input mode on the left is $m = 3$, $n = 1$. Contours are typical for a well cut on input mode.

transmission matrices are given here. 3×3 reflection and transmission matrices are investigated by considering input radial modes $n = 1$, 2, and 3. At $x = 0$ the two propagating modes and one cut-off mode have cut-off ratios $\xi = 2{\cdot}40$, $1{\cdot}26$, $0{\cdot}89$ respectively. At $x = L$, the single propagating mode and two cut-off modes have cut-off ratios $\xi = 1{\cdot}65$, $0{\cdot}87$, $0{\cdot}61$. An interesting feature of this geometry and flow is that mode $n = 2$ makes a transition from cut on to cut off in going from left to right. Mode $n = 3$ is deeply cut off at $x = L$.

Figure 7 shows acoustic iso-pressure contours for the case of nominal flow (left to right) with the mode $n = 1$ input at $x = 0$. The contours are consistent with a well cut on mode and significant scattering. Figure 8 shows contours for the case of reverse flow (right to left) with the source at the end $x = L$, and the input mode $n = 3$. This mode is deeply cut off and it should be noted how rapidly the acoustic pressure levels decay away from the source plane. It can be concluded that this mode effectively produces no acoustic pressure at $x = 0$.

Tables 9–12 are presented to verify the predicted reciprocal characteristics of the scaled acoustic potential reflection and transmission coefficients. Tables 9 and 10 show the scaled pressure reflection coefficients for nominal flow (left to right) and reverse flow (right to left) with the source at $x = 0$. These correspond with the left- and right-hand sides of equation (5). The reflection matrices shown in these two tables are seen to be reciprocals, as predicted.

Tables 11 and 12 show the scaled potential transmission coefficients for nominal flow (left to right) with the source plane at $x = 0$ and reverse flow (right to left) with the source at $x = L$. These correspond with the left- and right-hand sides of equation (7). The reflection matrices shown in these two tables are seen to be reciprocals for modes $n = 1, 2$. Reciprocity involving mode $n = 3$ seems to fail. The reason for this can be deduced by referring back to Figure 8 and noting that the deeply cut-off mode $n = 3$ creates acoustic pressure levels at $x = 0$ which are probably unresolvable with accuracy by the numerical model. To test this

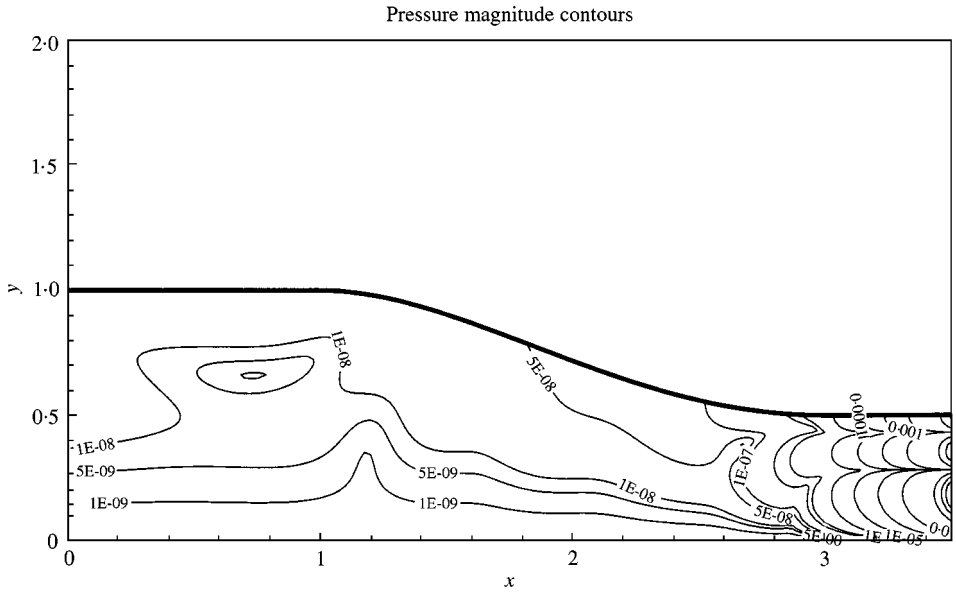

Figure 8. Acoustic iso-pressure contours for acoustically treated converging circular duct with reverse flow. At $x = 0$ the Mach number is $M_0 = -0{\cdot}13$ and at $x = L$ the Mach number is $M_L = -0{\cdot}71$. The non-dimensional frequency is $\eta_r = 10{\cdot}0$, and the input mode on the right is $m = 3$, $n = 3$. Contours are typical for a deeply cut off input mode.

TABLE 9

Scaled acoustic potential refelection coefficients for direct flow and source at $x = 0$ for the converging circular acoustically treated duct which corresponds to the left-hand side of equation (5). $\eta_r = 10$, $m = 3$

Mode	1	2	3
1	0·16566 + 0·11529 i	0·23310 + 0·05472 i	− 0·00056 − 0·00099 i
2	0·20720 + 0·09263 i	− 0·02814 + 0·01965 i	0·00035 − 0·00035 i
3	− 0·00044 − 0·00067 i	− 0·00069 − 0·00111 i	− 0·291(− 4) + 0·286(− 5) i

TABLE 10

Scaled acoustic potential reflection coefficients for reverse flow and source at $x = 0$ for the converging circular acoustically treated duct which corresponds to the right-hand side of equation (5). $\eta_r = 10$, $m = 3$

Mode	1	2	3
1	0·16566 + 0·11529 i	0·20720 + 0·09623 i	− 0·00044 − 0·00067 i
2	0·23310 + 0·05472 i	− 0·02814 + 0·01965 i	− 0·00069 − 0·00111 i
3	− 0·00056 − 0·00099 i	0·00035 − 0·00035 i	− 0·291(− 4) + 0·286(− 5) i

TABLE 11

Scaled acoustic potential transmission coefficients for direct flow and source at $x = 0$ for the converging circular acoustically treated duct which corresponds to the left-hand side of equation (7). $\eta_r = 10$, $m = 3$

Mode	1	2	3
1	$-0{\cdot}18538 + 0{\cdot}24017$ i	$0{\cdot}04016 + 0{\cdot}13443$ i	$-0{\cdot}223(-5) - 0{\cdot}286(-6)$ i
2	$0{\cdot}374(-4) - 0{\cdot}570(-4)$ i	$-0{\cdot}115(-4) - 0{\cdot}288(-4)$ i	$0{\cdot}110(-8) - 0{\cdot}344(-8)$ i
3	$-0{\cdot}521(-7) + 0{\cdot}116(-6)$ i	$0{\cdot}301(-7) - 0{\cdot}507(-7)$ i	$0{\cdot}260(-11) + 0{\cdot}595(-11)$ i

TABLE 12

Scaled acoustic potential transmission coefficients for reverse flow and source at $x = L$ for the converging circular acoustically treated duct which corresponds to the left-hand side of equation (7). $\eta_r = 10$, $m = 3$

Mode	1	2	3
1	$-0{\cdot}18538 + 0{\cdot}24017$ i	$0{\cdot}374(-4) - 0{\cdot}570(-4)$ i	$-0{\cdot}521(-7) + 0{\cdot}116(-6)$ i
2	$0{\cdot}04016 + 0{\cdot}13443$ i	$-0{\cdot}115(-4) - 0{\cdot}288(-4)$ i	$0{\cdot}301(-7) + 0{\cdot}507(-7)$ i
3	$0{\cdot}00014 - 0{\cdot}00005$ i	$0{\cdot}332(-7) + 0{\cdot}961(-8)$ i	$-0{\cdot}644(-10) - 0{\cdot}770(-11)$ i

hypothesis, another test of reciprocity with the same geometry, flow, and mode number was carried out, but with the non-dimensional frequency increased to $\eta_r = 12$ (from $\eta_r = 10$). This changes the cut-off ratios for the modes $n = 1, 2, 3$ to $\xi = 2{\cdot}88, 1{\cdot}51, 1{\cdot}07$ at $x = 0$ and $\xi = 1{\cdot}98, 1{\cdot}04, 0{\cdot}73$ at $x = L$. This makes three propagating modes at the left end and two propagating modes at the right end, and retains the interesting feature of the transition from cut on to cut off for mode $n = 3$ in a transition from left to right, or from cut off to cut on in the opposite direction.

Figure 9 shows acoustic iso-pressure contours for the case of reverse flow, with the source at the right end with $n = 3$ and $\eta_r = 12$. The contour levels show that at the left end the acoustic pressure levels are substantially higher than those shown in Figure 8, and they are more accurately resolved by the modelling scheme.

Tables 13 and 14 show the scaled potential transmission coefficients for nominal flow (left to right) with the source plane at $x = 0$ and reverse flow (right to left) with the source at $x = L$. The non-dimensional frequency is $\eta_r = 12$. Now reciprocity is satisfied (a reciprocal relationship of the scaled transmission matrices) to a high level of accuracy. It is concluded that the problem encountered at non-dimensional frequency $\eta_r = 10$ is caused by the lack of accurate resolution of the acoustic field of the deeply cut-off mode $n = 3$. This warns that there is a practical limit beyond which reciprocity may not be verifiable for cut-off modes.

A final example considers the converging circular duct profile previously shown in Figure 6 with the same steady flow Mach number, but in this case treated as one dimensional. Inlet and exit Mach numbers for the nominal flow are $M = 0{\cdot}13$ and $0{\cdot}71$. Acoustic propagation is also taken to be one dimensional at non-dimensional frequency $\eta_r = 1{\cdot}0$ based on a reference length which is the radius (of an assumed circular cross section) of the duct at the nominal source plane $x = 0$. This scaling makes everything

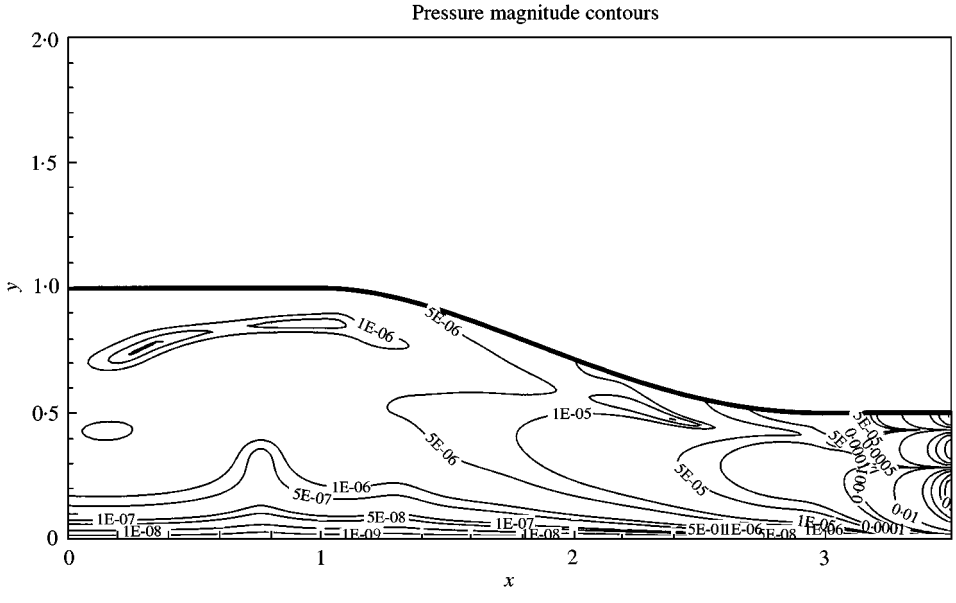

Figure 9. Acoustic iso-pressure contours for acoustically treated converging circular duct with reverse flow. At $x = 0$ the Mach number is $M_0 = -0{\cdot}13$, and at $x = L$ the Mach number is $M_L = -0{\cdot}71$. The non-dimensional frequency is $\eta_r = 12{\cdot}0$, and the input model on the right is $m = 3$, $n = 3$. Contours are typical for a moderately cut off input mode.

TABLE 13

Scaled acoustic potential transmission coefficients for direct flow and source at $x = 0$ for the converging circular acoustically treated duct which corresponds to the left-hand side of equation (7). $\eta_r = 12$, $m = 3$

Mode	1	2	3
1	$-0{\cdot}08862 + 0{\cdot}41280$ i	$0{\cdot}31074 - 0{\cdot}05362$ i	$0{\cdot}03674 + 0{\cdot}06580$ i
2	$-0{\cdot}02353 - 0{\cdot}00062$ i	$0{\cdot}02811 - 0{\cdot}03804$ i	$0{\cdot}00839 - 0{\cdot}00304$ i
3	$0{\cdot}877(-5) - 0{\cdot}791(-5)$ i	$0{\cdot}0255(-5) + 0{\cdot}237(-4)$ i	$-0{\cdot}208(-5) + 0{\cdot}397(-5)$ i

TABLE 14

Scaled acoustic potential transmission coefficients for reverse flow and source at $x = L$ for the converging circular acoustically treated duct which corresponds to the left-hand side of equation (7). $\eta_r = 12$, $m = 3$

Mode	1	2	3
1	$-0{\cdot}08862 + 0{\cdot}41280$ i	$-0{\cdot}02353 - 0{\cdot}00062$ i	$0{\cdot}877(-5) - 0{\cdot}791(-5)$ i
2	$0{\cdot}31074 - 0{\cdot}05362$ i	$0{\cdot}02811 - 0{\cdot}03804$ i	$0{\cdot}255(-5) + 0{\cdot}237(-4)$ i
3	$0{\cdot}03674 + 0{\cdot}06580$ i	$0{\cdot}00839 - 0{\cdot}00304$ i	$-0{\cdot}208(-5) + 0{\cdot}397(-5)$ i

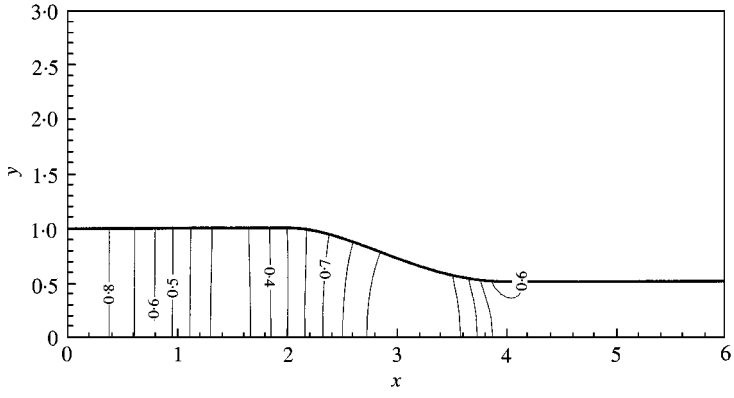

Figure 10. Acoustic iso-pressure contours for converging circular duct with nominal flow. At $x = 0$ the Mach number is $M_0 = 0{\cdot}13$, and at $x = L$ the Mach number is $M_L = 0{\cdot}71$. The non-dimensional frequency is $\eta_r = 1{\cdot}0$. The source is on the left and is input as $m = 0$, $n = 1$. This simulates and compares with one-dimensional propagation.

consistent with the axially symmetric duct formulation. Propagation at the chosen frequency has been modelled by the axially symmetric formulation using angular mode $m = 0$ and radial mode $n = 1$. Iso-potential contours for the steady flow are shown in Figure 6 and iso-acoustic pressure contours are shown in Figure 10 (with longer uniform extensions at the two ends, as compared to Figure 6). Due to the duct contour and steady flow, there is noticeable deviation from true one-dimensional propagation, however, there is no indication of substantial scattering into higher order modes, which the one-dimensional theory necessarily excludes.

Table 15 is a summary of the reciprocity and power invariance benchmark tests which are available in the one-dimensional case. The results of (a) and (b) substantiate the reciprocity statement of equation (9) and the results of (c) and (d) substantiate the reciprocity statement of equation (11). The power results (e)–(l) substantiate the observations based on power considerations that power reflection and transmission coefficients are independent of flow direction and source location (equations (13) and (14)). As an indication of the comparison between the axially symmetric (3-D) duct model and the one-dimensional model, power reflection and transmission coefficients for the axially symmetric model are also shown. The invariance of the power transmission and reflection coefficients to flow direction and source location is true (numerically) at low frequencies in the axially symmetric duct and the one-dimensional predictions of reflection and transmission characteristics quite favorably correlate with predictions of the axially symmetric model. The properties of invariance of the power reflection and transmission coefficients is not generally true at higher frequencies in the axially symmetric model when scattering into higher or lower modes occurs.

4. CONCLUSION

Numerical verification of the reciprocal relationships derived in reference [1] has been accomplished using a finite element model for duct propagation. Three cases have been presented for an axially symmetric duct model, one introducing the feature of transition from an annular to a circular duct without and with acoustic treatment, and the second introducing a converging duct with substantial steady flow acceleration and

TABLE 15

Summary of scattering matrix reciprocity and power invariance benchmark tests for a one-dimensional converging duct, with power invariacne comparisons for an axially symmetric model. $M_0 = 0{\cdot}13, M_L = 0{\cdot}71, \eta_r = 1{\cdot}0$ ($m = 0, n = 1$ *in the axially symmetric case*)

Coefficient	3-D	1-D	1-D
(a) Reflection coefficient, direct flow, source left			0·430129 + 0·050053 i
(b) Reflection coefficients, reverse flow, source left			0·430129 + 0·050053 i
(c) Scaled transmission coefficient, direct flow, source left			0·384607 + 0·145370 i
(d) Scaled transmission coefficient, reverse flow, source left			0·384607 + 0·145370 i
(e) Power reflection coefficient, direct flow, source left:	0·171105	0·187517	
(f) Power reflection coefficient, reverse flow, source left	0·171105	0·187517	
(g) Power reflection coefficient, direct flow, source right	0·171105	0·187517	
(h) Power reflection coefficient, reverse flow, source right	0·171105	0·187517	
(i) Power transmission coefficient, direct flow, source left	0·828895	0·812483	
(j) Power transmission coefficient, reverse flow, source left	0·828895	0·812483	
(k) Power transmission coefficient, direct flow, source right	0·828895	0·812483	
(l) Power transmission coefficient, reverse flow, source right	0·828895	0·812483	

segmented acoustic treatment. A fourth case is presented for the converging duct at low frequency where a one-dimensional model of propagation is appropriate. Reciprocal characteristics of the scattering matrices are verified with exceptional accuracy, as are predicted relationships for power reflection and transmission coefficients in the one-dimensional case.

REFERENCES

1. W. EVERSMAN 2001 *Journal of Sound and Vibration* **246**, 71–95. A reverse flow theorem and acoustic reciprocity in compressible potential flows in ducts.
2. S. S. DAVIS 1976 *Journal of the Acoustical Society of America* **59**, 264–266. On an invariance property of acoustic waveguides.
3. W. EVERSMAN 1979 *Journal of Sound and Vibration* **47**, 515–521. A reciprocity relationship for transmission in non-uniform hard walled ducts without flow.
4. W. MOEHRING 1978 *Journal of the Acoustical Society of America* **64**, 1186–1189. Acoustic energy flux in nonhomogeneous ducts.
5. W. MOEHRING 2000 *Journal of Fluid Mechanics* **431**, 223–237. Energy conservation, time reversal invariance and reciprocity in ducts with flow.
6. M. K. MYERS 1980 *Journal of Sound and Vibration* **71**, 429–434. On the acoustic boundary condition in the presence of flow.

7. I. DANDA ROY and W. EVERSMAN 1995 *American Society of Mechanical Engineers, Journal of Vibration and Acoustics* **117**, 109–115. Improved finite element modeling of the turbofan engine inlet radiation problem.
8. W. EVERSMAN and D. OKUNBOR 1998 *Journal of Sound and Vibration* **213**, 235–257. Aft fan duct acoustic radiation.
9. W. EVERSMAN 2001 *Journal of Sound and Vibration* **246**, 63–69. The boundary condition at an impedance wall in a nonuniform duct with potential mean flow.